Glued-in rods for timber structures - a 3D model and finite element parameter studies

Serrano, Erik

Published in:
International Journal of Adhesion and Adhesives

DOI:
10.1016/S0143-7496(00)00043-9

2001

Glued-in Rods for Timber Structures
– A 3D Model and Finite Element Parameter Studies

Erik Serrano
Division of Structural Mechanics, Lund University
PO Box 118, SE-221 00 Lund, Sweden

Submitted for publication in International Journal of Adhesion and Adhesives

Abstract A nonlinear 3D finite element model and a parameter study in relation to glued-in rods for timber structures are presented. A strain-softening crack band model was used to characterise the behaviour of the adhesive layer between the rod and the wood. The model is general in the sense that it bridges the gap between the theory of an ideal plastic bondline and the theory of linear elastic fracture mechanics. Two parameter studies were made. One in relation to fracture energy and geometrical parameters and the second in relation to loading conditions. The results show that the fracture energy is of major importance for the pull-out load capacity, that the present model can be used to predict such phenomenon like the size effect and that the loading in pull-compression results in lower load-bearing capacities than the loading in pull-pull.

Keywords: wood, fracture, finite element method, glued-in rod

1 Introduction

1.1 Background

Glued-in rods are used primarily for two purposes in timber engineering: either as a connector between structural elements or as a reinforcement of the wood in areas of high stresses perpendicular to the grain, such as around holes and notches and in the apex zone of curved and tapered beams. As

connectors, glued-in rods have been used, especially for glued-laminated timber (glulam), for many years – in Europe mainly in the Nordic countries and in Germany. The glued-in rod connection makes it possible to obtain strong and stiff joints with excellent performance in load transfer without the disturbing appearance of the large metal plates often used for other connector types. Another advantage is the good fire resistance, since the connection is embedded in the insulating wood.

This paper reports some results from a part of a European research project, "GIROD–Glued-in Rods for Timber Structures" which has been running since 1998. The project aims at developing new design equation proposals for glued-in rods. The need for such design equations in the European codes was pointed out by Aicher and Herr in [1]. They showed that the present design *recommendation* to the annex of the European standard (EC5), ENV 1995-Part 2 Bridges, is questionable. The EC5-equation assumes that the nominal shear strength at pull-out of a glued-in rod is independent of the rod's size (diameter as well as anchorage length). Aicher and Herr showed that on the basis of test data taken from the literature and from a new test series, the EC5-equation gives approximately two times higher design values of the pull-out load than the test results indicate.

In the GIROD project, the work is concentrated on the prediction of the pull-out strength of *axially* loaded glued-in rods. The rods used are threaded steel rods of different diameters and glued-in lengths, and rods of glass-fibre reinforced polyester. All rods are glued into the glulam in holes with a diameter which is 1 mm larger than the nominal diameter of the rod. Three different adhesives are included in the project: a fibre reinforced phenol-resorcinol, a 2-component polyurethane and an epoxy. A schematic of the GIROD test specimens and the geometry of the model used for the numerical simulations in the present study are shown with some main notations in Figure 1.

In the numerical model of the present study, it has been assumed that a symmetry plane exists at half the specimen length, since it is reasonable to assume that at some distance from the glued-in end of the testing rod, the wood is in a state of uniaxial tensile strain.

1.2 Previous Work

Experimental

The performance of glued-in rods in timber has been investigated experimentally by several researchers in the past. These investigations mainly concern glued-in bolts or reinforcement bars, glued into glulam. Threaded steel bolts

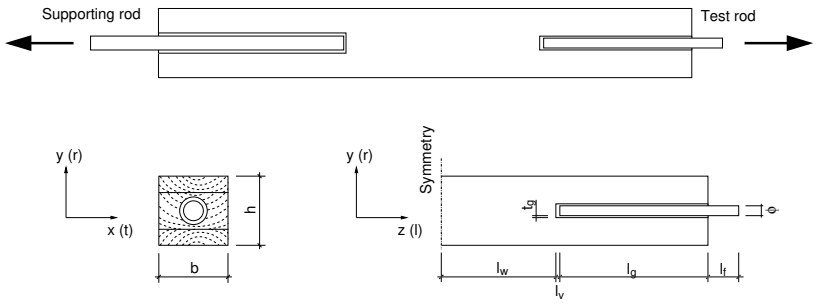

Figure 1: Schematic of test specimens and model used for simulations.

were tested by Riberholt [2], by Ehlbeck and Siebert [3] and recently by Deng [4], Aicher and Herr [1], and Aicher et al. [5]. Tests on glued-in, ribbed, reinforcement bars were performed by Kangas [6] and Korin [7]. The adhesives used in these experimental investigations are epoxies, polyurethanes or resorcinol/phenolic adhesives. In [8], a large number of potential adhesives for glued-in rods are tested.

The results from all these investigations show that the shear strength of glued-in rods is influenced by the anchorage length, i.e. the axial load resistance is not proportional to the glued-in length. Both Riberholt [9] and Kangas [6] derived design equations in which the effect of the anchorage length was taken into account. For example Riberholt [9], proposes a design equation for the axial load capacity, P_u, according to:

$$P_u = k\rho d\sqrt{l_g} \tag{1}$$

where k is a material constant, different for different adhesives, ρ is the wood density, d is the bolt diameter and finally l_g is the glued-in length (anchorage length). This equation was derived on a purely empirical basis by curve fitting of the experimental results. This result is typical for the design equations found in the literature with the pull-out load given by a nonlinear function of the material and geometrical parameters. The expression found in Eurocode 5 in contrast assumes a relation according to:

$$P_u = f_v \pi d_{equ} l_g \tag{2}$$

with f_v being the equivalent shear strength of the wood, which is given by:

$$f_v = 1.2 \cdot 10^{-3} d_{equ}^{-0.2} \rho^{1.5}, \quad d_{equ} = min\{d_h, 1.25d\} \tag{3}$$

Here d_h is the hole diameter and d is the nominal diameter in the case of threaded rods. These equations give as a result a pull-out strength that is

slightly influenced by the diameter of the rod, not at all influenced by the glued-in length and finally very much influenced by the wood density.

Analytical

Several theoretical bases could be used for the development of calculation models for the pull-out of glued-in rods, the most trivial one being the assumption of a uniform shear stress distribution along the entire rod. Such a model can be expected to work well for small glued-in lengths and ductile adhesives, but is not realistic for design purposes. The glued-in lengths used in practice will result in non-uniform stress distributions, [3, 10, 11, 12].

A linear elastic stress analysis using the traditional Volkersen assumptions [13], is one way to take into account the non-uniform stress distribution. However, since large stress gradients are common, the post-peak stress behaviour of the bondline is essential and consequently a linear elastic stress analysis is of little use.

To take into account the large stress gradients, an approach based on the assumptions of linear elastic fracture mechanics (LEFM) can be used to develop a design equation. Such an approach will be accurate for cases of large glued-in lengths, in which case the fracture process region is small compared to the other dimensions of the structure.

A theory which includes the two extremes of a perfectly plastic behaviour and the brittle behaviour according to LEFM is the so-called generalised Volkersen theory, developed by Gustafsson [14]. Based on this theory, a rational expression for the pull-out of a glued-in rod was derived by Johansson et al. [11]. The generalised Volkersen theory takes into account the fracture-softening capabilities of the bondline by introducing the fracture energy in the constitutive equations. Instead of using the linear elastic shear modulus of the adhesive layer, an equivalent stiffness defined in terms of the fracture energy and the bondline thickness is used. The expression for the ultimate pull-out load, P_u, reads:

$$P_u = f_v d\pi l_g \frac{(1+\alpha)\sinh\beta}{\beta((\alpha+\cosh\beta)\cosh\beta-\sinh^2\beta)} \tag{4}$$

$$\beta = \sqrt{\frac{1+\alpha}{2}}\sqrt{\frac{l_g^2 f_v^2 d\pi}{(EA)_{wood}G_f}}, \quad \alpha = \frac{(EA)_{wood}}{(EA)_{rod}} > 1 \tag{5}$$

where f_v is the shear strength of the adhesive layer, d is the bolt diameter, l_g is the glued-in length, α is the axial stiffness ratio of the adherends, $(EA)_{wood}/(EA)_{rod}$, with E denoting the Young's moduli in the axial direction and A the respective cross-sectional areas and, finally, G_f is the fracture

energy of the adhesive layer. A corresponding expression was also set up for the case of $\alpha \leq 1$. For small values of β, Eq. (4) coincides with the theory of a perfectly plastic bondline, i.e. the pull-out load is determined by the glued-in length and diameter of the rod, and the strength of the bondline. For large values of β, the pull-out load is determined by the fracture energy of the bondline, the stiffness of the adherends and the square root of the absolute size of the structure.

Numerical

An early example of using finite elements in the modelling of glued-in rods is the work by Müller and Roth [12]. They used a rather coarse FE-mesh to examine the linear elastic stress distribution and its dependence on some geometrical parameters. Later, larger models have been presented, e.g. by Aicher et al. in [10, 15], used for stress distribution analyses and heat transfer simulations. A somewhat more complex modelling approach was used by Guan [16], who used a built-in stress-based debonding feature of the FE-code combined with a contact algorithm to model the failure of the adhesive layer and the interaction between the failure surfaces. A nonlinear modelling with a bondline model tailor-made for wood adhesive bonds was presented by Johansson et al. in [11]. Here the strain-softening capabilities of the bondline was taken into account and the progressive failure of a glued-in rod was modelled. As in the other numerical studies, a two-dimensional, axisymmetric, model was used.

In evaluating the numerical results, some previous results from Gustafsson [14] relating to the use of a nonlinear fracture mechanics (NLFM) approach will be used. By the theory of NLFM is meant a theory based on a cohesive crack model, e.g. a fictitious crack model (FCM) or a crack band model (CBM), which can take into account strain softening and progressive crack growth.

From the one-dimensional theory of NLFM, a characteristic length, l_{ch}, of a material can be defined by:

$$l_{ch} = \frac{EG_f}{f_f^2} \tag{6}$$

where E is the stiffness, G_f the fracture energy and f_f the strength of the material. The characteristic length is a measure of the brittleness of the material and also a measure of the size of the fracture process zone. A brittleness ratio, ω, of a structure can be defined in terms of its size normalised

with respect to the characteristic length:

$$\omega = \frac{d}{l_{ch}} = \frac{d\, f_f^2}{EG_f} \tag{7}$$

where d is a typical dimension of the structure. The brittleness ratio ω defined by Eq. (7) has been used for parameter studies using a FCM, see e.g. [17]. It is now possible, [14], to express the load-bearing capacity in a dimensionless form if all geometrical and material properties are normalised. This means that in a parameter study, a change in material stiffness must be made proportional for all the materials in the model, the geometrical shape of the structure must not be changed and the nonlinear response of the strain softening material must have an unchanged normalised shape. This normalised shape can be defined in several ways and the definition used in the present study is described in the results section. Using normalised parameters, the load-bearing capacity of the structure in dimensionless form is given by a nonlinear function of ω only:

$$\bar{\tau} = \mathcal{F}(\omega) \tag{8}$$

where $\mathcal{F}$ denotes an unknown function. According to [14] there are bounds on $\frac{d\mathcal{F}}{d\omega}$:

$$-0.5 < \frac{d\mathcal{F}}{d\omega} < 0. \tag{9}$$

The bounds coincide with the linear elastic fracture mechanics theory for $\frac{d\mathcal{F}}{d\omega} = -0.5$ and the theory of perfect plasticity for $\frac{d\mathcal{F}}{d\omega} = 0$. These bounds are useful for checking a numerical implementation of FCM-like models for the cases of extremely brittle or extremely ductile behaviour.

1.3 Failure Modes

All the previously mentioned investigations regard the failure of a glued-in rod as being determined by the pull-out of the rod, with a shear failure in the adhesive/rod interface, in the wood/adhesive interface or in the wood close to the bondline. However, if the edge distance is short, splitting failure of the wood will determine the strength of the connection. The splitting failure is caused by tensile stresses perpendicular to the wood grain. An early design proposal by Möhler and Hemmer [18] states that the minimum edge distance should be 4 times the nominal diameter of the rod. Riberholt [9] proposed the minimum edge distance to be 1.5–2.5 times the rod diameter if the adhesion to the rod is good and 2.5–4 times the diameter for the case of bad adhesion to the rod.

In the experimental investigation conducted by Deng [4], the splitting failure proved to be the dominating one. In this study however the edge distances were 1.5–2.25 times the diameter of the rod and the failure often located at the rod/adhesive interface.

1.4 Present study

The present paper presents a 3D nonlinear model developed for the prediction of the pull-out strength of glued-in rods. Results from a FE parameter study of factors affecting the strength of such rods are also presented. Two different parameter studies with somewhat different objectives are presented:

I influence of various geometry and material properties on the pull-out strength

II influence of the loading conditions on the pull-out strength

The results from the FE calculations in study I are compared with hand calculation formulas based on the classic theory of strength of materials, linear elastic fracture mechanics and the generalised Volkersen theory. At present, the computational model has not been calibrated to actual test results, since input data for the bondline model are not yet available.

2 Computational Model

2.1 General Remarks

All simulations have been performed with three-dimensional finite elements using the general purpose finite element code ABAQUS [19]. The model of a specimen consists of three materials: wood, bondline and steel. The wood and the steel parts are treated as linear elastic continua, while the bondline is modelled as a layer in which the shear stresses and the peel stress are nonlinear functions of the relative shear and normal displacements across the layer. The bondline model was implemented using an option of the FE-code allowing a user-defined material to be included in the analysis.

The failure of the glued-in rod is assumed to take place within or in the vicinity of the adhesive layer. The input for the present bondline model is the stress-slip performance of the adhesive layer. It is assumed that such a stress-slip performance can be recorded for a small specimen in a stable pull-out test. A stable test is a test that includes the strain-softening branch of the stress-slip curve. It is then possible to calibrate the input data for

Table 1: Adopted material parameters for the wood.

Young's modulus		Shear modulus		Poisson's ratio	
E_t	500	G_{tr}	60	ν_{tr}	0.3
E_r	800	G_{tl}	700	ν_{tl}	0.02
E_l	14000	G_{rl}	600	ν_{rl}	0.02

the bondline model in such a way that the test results can be reproduced in a numerical finite element simulation. If the mode of failure for such a test is equal to the failure mode expected for structural-sized glued-in rods, the assumption is that the present modelling is accurate. In this sense the bondline model is a model for the adhesive itself as well as for the boundary layers on either side of it.

Steel rods used in timber connections are often threaded, but this threading is not modelled in detail in the present study. The effect of the threading is twofold: firstly it may give a different response of the bondline compared to a smooth rod of the same diameter and, secondly, it reduces the axial stiffness compared to a smooth non-threaded rod of the same diameter.

2.2 Material Modelling

Wood and Steel

The wood is modelled as being a linear elastic orthotropic material. The influence of taking into account the actual annual ring curvature of the timber, shown schematically in Figure 1, was investigated but it was found to have a negligible effect on the results, and therefore the material directions were assumed to be constant in the timber. The numerical values of the elastic parameters that have been used are given in Table 1 (t = tangential, r = radial and l = longitudinal direction (MPa))

The steel rods are modelled as being linear elastic and isotropic. The Young's modulus is set to 210 000 MPa and the Poisson's ratio $\nu = 0.3$.

Bondline Model

The strain-softening bondline model used is a further development of a model by Wernersson [20], and applied by Serrano and Gustafsson [21]. The original model was two-dimensional and developed for thin bondlines which were assumed to fail along a line of failure, involving only one shear-stress component

and the peel stress of the bondline. An expansion of this model was made for the present study so that it now involves the two shear-stress components and the peel-stress component of an assumed plane of failure. Thereby the model can be used for adhesive layers in three-dimensional structures.

The behaviour of the bondline is defined by piecewise linear curves, describing the uniaxial behaviour for shear stress vs. shear slip (2 curves) and peel stress vs. normal displacement. Assuming a piecewise linear relation is the simplest way of obtaining a good fit to experimental data, yet making it possible to fit complicated response curve shapes. In the present study piecewise linear relations with three segments are used. An example of such a piecewise linear curve is given in Figure 2.

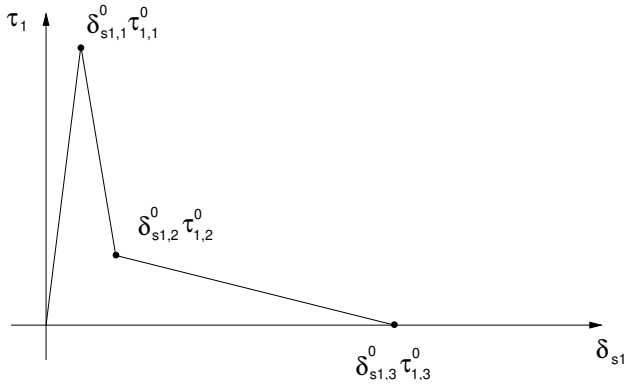

Figure 2: Stress-slip curve for a bondline in uniaxial shear.

The stress-strain relations in the bondline plane directions are assumed to be linear elastic. The three stress components in these directions (two normal and one shear stress) are not considered in the fracture model.

A general mixed-mode state of deformation of the bondline is given by two shear-slip deformations $(\delta_{s1}, \delta_{s2})$ and by the normal deformation across the bondline (δ_n). The bondline response is assumed to retain its piecewise linear shape for radial deformation paths (constant ratio $(\delta_{s1} : \delta_{s2} : \delta_n)$), but vary smoothly with the degree of mixed mode, expressed by the mixed mode angles φ_{ss} and φ_{sn}:

$$\varphi_{ss} = \arctan \frac{\delta_{s1}}{\delta_{s2}} \tag{10}$$

$$\varphi_{sn} = \arctan \frac{\delta_s}{\delta_n} \tag{11}$$

$$\delta_s = \sqrt{\delta_{s1}^2 + \delta_{s2}^2} \tag{12}$$

The following criterion is used to determine whether the current state of deformation is elastic or not:

$$(\frac{\delta_{s1}}{\delta^0_{s1,1}})^{m1} + (\frac{\delta_{s2}}{\delta^0_{s2,1}})^{m2} + (\frac{\delta_n}{\delta^0_{n,1}})^p \leq 1 \tag{13}$$

In Eq. (13) $s1$ and $s2$ correspond to the two directions in a plane of failure. Subscript n refers to the peel response, subscript 1 refers to the first breakpoint of the piecewise linear curve and finally, superscript 0 stands for the uniaxial properties.

If the current state is elastic, according to Eq. (13), the response is linear and uncoupled, according to the uniaxial responses. If not, the current state of mixed mode is calculated according to Eq. (10)–(11). Following this, the new deformations ($\delta_{s1,i}$, $\delta_{s2,i}$ and $\delta_{n,i}$) corresponding to the breakpoints on the piecewise linear curve are calculated with an expression analogous to Eq. (13). The stresses corresponding to each such breakpoint, i, are then calculated according to:

$$\tau_{1,i} = \tau^0_{1,i} \cdot \frac{\delta_{s1,1}}{\delta^0_{s1,1}} \tag{14}$$

$$\tau_{2,i} = \tau^0_{2,i} \cdot \frac{\delta_{s2,1}}{\delta^0_{s2,1}} \tag{15}$$

$$\sigma_i = \sigma^0_i \cdot \frac{\delta_{n,1}}{\delta^0_{n,1}} \tag{16}$$

Knowing the stresses at the breakpoints, the stress for the current state of deformation can be obtained by linear interpolation. In FE-analysis, it is necessary not only to define the state of stress for the current state of deformation, but also to give the tangential stiffness of the material for this state, i.e. the derivative of the stress with respect to the strains. In the current implementation this is performed numerically, since for the present material model it is very difficult to obtain a general explicit equation for the derivative. The above model is concentrated on the severe state of simultaneously acting peel and shear stresses. For the case of a compressive stress perpendicular to the bondline, the shear stress-slip behaviour is assumed to coincide with the uniaxial response, and the normal stress-displacement behaviour is assumed to be linear elastic.

In the FE-implementation of the above model, a so-called crack band approach has been used. This means that the above stress-displacement relations are transformed into corresponding stress-strain relations by dividing the displacements by the thickness of the continuum finite element used to model the bond layer. This results in a material length being introduced as

a material property apart from the uniaxial stress-strain relations and the powers *m1, m2, p* of Eq. (13).

In the present study it has been assumed that

$$m1 = m2 = p = 2. \tag{17}$$

The tri-linear stress-displacement relation is defined through

$$\tau^0_{1,2} = \tau^0_{1,1}/3, \quad \tau^0_{1,3} = 0. \tag{18}$$

Furthermore

$$\delta^0_{s1,2} = 4\delta^0_{s1,1}, \quad \delta^0_{s1,3} = 40\delta^0_{s1,1}. \tag{19}$$

The performance in the $s2$-direction was assumed to be the same as in the $s1$-direction. In the n-direction it was assumed that

$$\sigma^0_2 = \sigma^0_1/4, \quad \sigma^0_3 = 0. \tag{20}$$

It was further assumed that

$$\delta_{n,2} = 30\delta_{n,1}, \quad \delta_{n,3} = 180\delta_{n,1}. \tag{21}$$

The strengths in the three directions are given by

$$\tau_f = \tau^0_{1,1} = \tau^0_{2,1}, \quad \sigma_f = \sigma^0_1 \tag{22}$$

which together with the relations

$$G_{f,s} = \int \tau^0_1 d\delta^0_{s1} = \int \tau^0_2 d\delta^0_{s2}, \quad G_{f,n} = \int \sigma^0 d\delta^0_n \tag{23}$$

define the bond layer properties for the given numerical values of only four parameters: τ_f and σ_f for the strengths in shear and peel, and $G_{f,s}$ and $G_{f,n}$ for the corresponding fracture energies.

2.3 Load and Boundary Conditions

All loading was applied using displacement control in order to make it possible to trace possible post peak-load behaviour.

In all simulations, half the width of the specimen was analysed, implying symmetry at this section. Modelling half the width of the cross-section makes it possible to vary, for example, the material properties across the height. Otherwise, for the present case, with a square cross-section and material directions according to Figure 1, only 1/4 of the total cross-section would have to be considered.

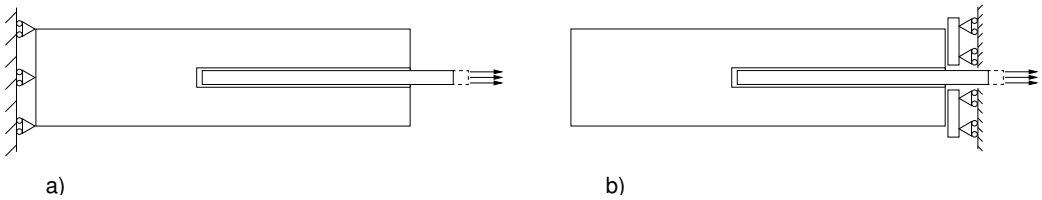

Figure 3: Loading of glued-in rod by a) "pull-pull" and b) "pull-compression"

In study I, the load was applied by "pull-pull", Figure 3a. In study II, the load was also applied by "pull-compression", Figure 3b. Here the face of the glulam in the vicinity of the rod was assumed to interact with a stiff loading plate, which in turn was prescribed to zero displacement. A contact algorithm available in the FE code was used to model the interaction between the wood and the loading plate, and the coefficient of friction was set to be 0.6.

2.4 Finite Element Model

The element subdivision used for most calculations is shown in Figure 4. The model consists of approximately 14000 nodes and 12000 elements. The bondline is modelled with 50 elements in the axial direction and 12 elements in the circumferential direction.

The elements representing the wood and the steel are standard isoparametric brick elements. The bondline was modelled using the same element type but with reduced integration (1 gausspoint) in order to avoid problems with the extreme slenderness ratio of the bondline elements.

For some of the calculations with extremely brittle adhesive properties, giving a small active fracture-process zone, the element subdivision along the rod was refined by increasing the number of elements from 50 to 100.

In order to check if the finite element subdivision in the plane of the cross-section was fine enough, a mesh consisting of approximately 65000 nodes (i.e. 195000 degrees of freedom) was used in one calculation. The difference in calculated load-bearing capacity compared with the 14000 nodes model was less than 1%.

For the simulations in study II involving contact modelling, the FE-discretisation was slightly changed to better fit the different plate geometries studied.

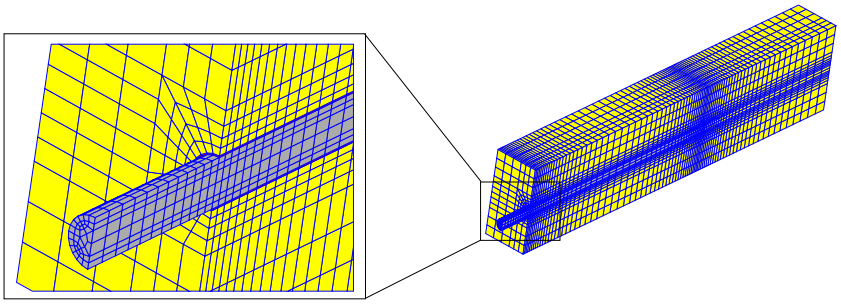

Figure 4: The FE-mesh used in the parameter studies.

3 Parameter Study I–Geometry and Material

3.1 Simulation Scheme

The different simulations performed are grouped into 6 different groups denoted A–F. Simulation A1 is the reference case, and each of the other groups involve simulations where parameters have been changed in relation to this case. The different groups of simulations involve:

A: Variation of fracture energies, G_f, at a constant ratio $G_{f,s}/G_{f,n} = 4$, keeping the strength of the bondline and the shape of the stress-slip curves unchanged. The results obtained here also give information about the effect of a proportional change of τ_f and σ_f, about the effect of a proportional change of all stiffness parameters of the wood and the steel, and about the effect of a proportional change of all geometrical dimensions (size effect), cf. Eq. (7).

B: Variation of lengths l_g and l_w at a constant ratio $l_g/l_w = 1.4$, thus changing the slenderness ratio l_g/ϕ of the rod.

C: Variation of the rod diameter, ϕ.

D: Variation of the length of solid wood, l_w.

E: Variation of the bondline strength. (τ_f in simulations E1-E2 and σ_f in simulations E3-E4).

F: Variation of cross-sectional dimensions, b and h at a constant ratio $b/h = 1.0$.

In the reference case, A1, the following numerical values of the geometry parameters were used (mm): $\phi = 16$, $t_g = 0.5$, $l_g = 320$, $l_w = 230$, $l_v = 3$, $b = 120$, $h = 120$. The numerical values used for the material parameters in the bondline were: $\tau_f = 12$, σ_f =4 (MPa), $G_{f,s} = 2000$, $G_{f,n} = 400$ (J/m^2). The numerical values used for the bondline are estimates based on test results from tests performed on wood to wood adhesive bonds [20] and from a preliminary study on the behaviour of glued-in bolts [11].

3.2 Results

The results from the simulations are summarised in Table 2. The table gives the changing input parameters in relation to the reference case and the results from the simulations in terms of the ultimate load, P_u, the mean shear stress at failure $f_v = P_u/(\pi\phi l_g)$, the normalised shear strength $\bar{\tau} = f_v/\tau_f = P_u/(\pi\phi l_g \tau_f)$ and the mean tensile stress in the rod $f_u = P_u/(\pi\phi^2/4)$. The possible failure of the steel rod in the simulations involving high values of fracture energy has not been accounted for since these simulations were performed to illustrate the capabilities of the bondline model.

Figure 5 shows the load-displacement response and Figure 6 shows the stress distributions along the bondline for the simulations A1, B1 and B2.

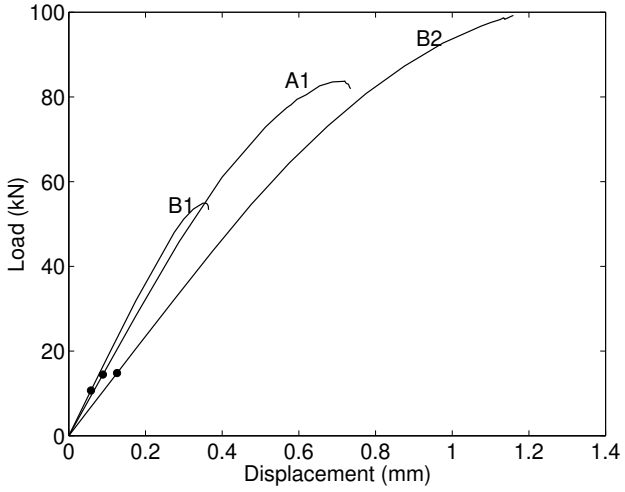

Figure 5: Load-displacement response from simulations A1, B1 and B2. The dots indicate the instance of fracture initiation.

The stress distributions are given for the centroid of the bondline elements closest to the symmetry plane, but since the state of deformation is very close to axisymmetric the shown distributions also apply, with negligible

Table 2: Results from simulations.

Name	Changing parameter and value	P_u (kN)	f_v (MPa)	$\bar{\tau}$ (-)	f_u (MPa)
A1	Reference	83.8	5.21	0.434	417
A2	$2G_f$	101.4	6.30	0.525	504
A3[a]	$0.5G_f$	65.9	4.09	0.341	327
A4	$4G_f$	121.4	7.55	0.629	604
A5[a]	$0.25\ G_f$	45.8	2.85	0.237	228
A6	$8G_f$	147.0	9.14	0.762	731
A7[a]	$0.125\ G_f$	33.6	2.09	0.174	167
A8	$16G_f$	171.6	10.7	0.889	853
A9	$32G_f$	184.1	11.4	0.954	916
B1	$0.5l_g$, $0.5l_w$	54.9	6.83	0.569	273
B2[a]	$2l_g$, $2l_w$	99.2	3.08	0.257	493
C1	0.5ϕ	33.0	4.10	0.342	657
C2	2ϕ	186.0	5.78	0.482	231
C3	0.25ϕ	12.1	3.02	0.251	963
D1	$0.5l_w$	82.1	5.10	0.425	408
D2	$0.25l_w$	84.4	5.24	0.437	420
E1	$0.5\tau_f$	60.7	3.78	0.629	302
E2[a]	$2\tau_f$	97.2	6.04	0.252	483
E3	$0.5\sigma_f$	83.7	5.21	0.434	416
E4	$2\sigma_f$	84.5	5.25	0.438	420
F1	$0.5b$, $0.5h$	91.9	5.71	0.476	457
F2	$2b$, $2h$	81.8	5.08	0.424	407

[a]Fine element subdivision used.

differences, for any other path along the rod. The stresses are given for two load levels of the tensile load, 5 kN and ultimate load. For all the cases, the 5 kN load level is within the linear elastic range. The plots are normalised with respect to the relative glueline coordinates, z/l_g.

The linear elastic stress distributions reveal that tensile peel stresses develop at the end where the load is applied ($z = 0$). For the simulations A1 and B2 the shear stress maximum also occurs at this end, while for simulation B1 it occurs at $z = l_g$. However, due to the tensile peel stresses, the fracture begins for all cases at $z = 0$. The stress distributions at ultimate load reveal that the bondline has started to soften at both ends for the simulations A1 and B1. For simulation B2 the bondline has started to soften only at $z = 0$ at ultimate load.

Based on results from a small test series reported by Johansson et al. [11], and from preliminary test data from the GIROD project, the estimated bondline fracture energy in shear is in the range of 2–10 kJ/m^2 depending on the type of adhesive. In this range the series A simulations show that the fracture energy is a parameter with a major influence on the pull-out strength. A doubling of the fracture energy results in an approximately 20% higher load-bearing capacity.

The simulations in series B give the expected effect of glued-in length on the nominal shear strength, f_v. The longer the glued-in length, the more non-uniform the stress distribution, thus lower values of f_v are obtained.

In simulations type C, the change of diameter of the rod also results in a different stress distribution. In the reference case, A1, the ratio of the axial stiffnesses, α, is rather high, about 4.7. Increasing the rod diameter will result in a value of α closer to unity and consequently a more uniform stress distribution ($\alpha = 1$ corresponds to a square wood cross-section of approximately 57 mm width and a rod of 16 mm diameter).

The simulations of series D were performed to check that the distance l_w has been chosen great enough not to cause any boundary effects.

In series E, the effect of performing a non-proportional change of the strength of the bondline in shear and in peeling was investigated. The results show that the dominating material strength is the shear strength of the bondline, in spite of the fact that the present model takes into account the shear strength reduction at a simultaneously acting peel stress. The linear elastic stress distributions include both peel stress and shear stress as shown in Figure 6. But after the fracture has occurred, the failure mode is dominated by pure shearing. Thus for the geometry of A1, the load level at which fracture begins is influenced strongly by the peel strength, but the ultimate load-bearing capacity is not affected to the same extent.

Series F, finally, shows the effect of changing the wood cross-section. The

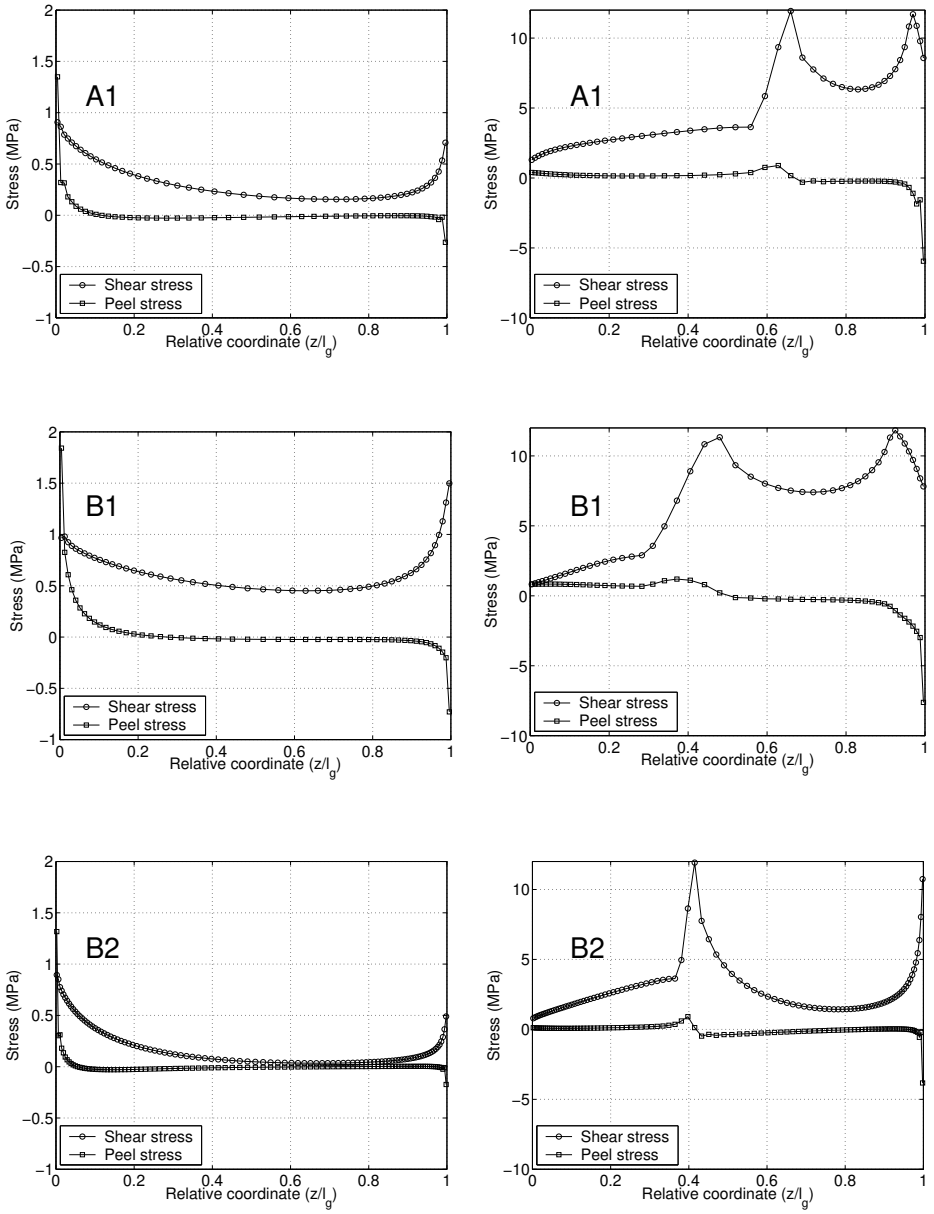

Figure 6: Linear elastic stress distributions at 5 kN global load (left) and stress distribution at ultimate load (right) for simulations A1, B1 and B2.

results can be explained in terms of axial stiffnesses and the stiffness ratio α, in line with the discussion above. Here a *larger* wood cross-section gives a *larger* value of α, and thus a more non-uniform stress distribution, compared to the reference case.

Now we turn again to the series A simulations using the dimensionless format previously discussed. The brittleness ratio, ω, was defined in Eq. (7) and is now used with $f_f = \tau, E = E_l, G_f = G_{f,s}, d = l_g$ to present the results from simulations A1–A9 in dimensionless form as $\bar{\tau}$ vs. ω. The normalised shape of the bondline response as discussed in relation with Eq. (8)–(9) is defined by $\tau_{s1}/\tau_{f,s1}$ and $\delta_{s1}/(G_f/\tau_{f,s1})$ for normalised stress and normalised deformation respectively. Figure 7 shows the results from simulations A1–A9 using this normalised format. The figure also illustrates the strength as

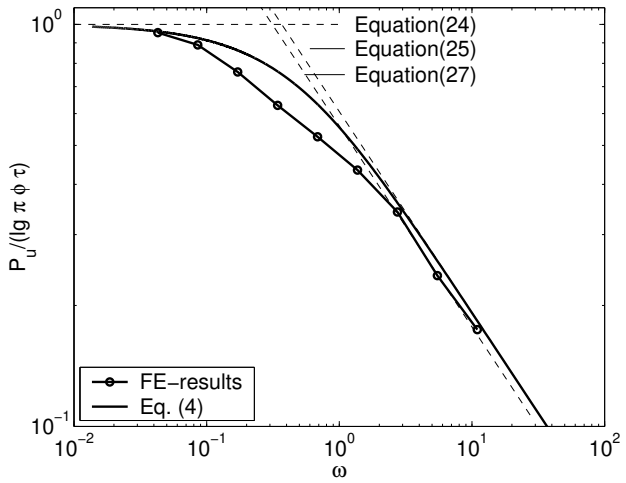

Figure 7: $\bar{\tau}$ vs. ω for simulations A1-A9 . Note the logarithmic scales.

predicted by the theory of perfect plasticity ($\bar{\tau} =$) constant = 1.0, and by the theory of linear elastic fracture mechanics $\bar{\tau} = C \cdot \omega^{-0.5}$, where C is a geometry (shape) constant and, finally, the strength predicted by Eq. (4). For the present case the following expressions apply, assuming that the bondline acts in pure shear and that the adherends act in pure tension:

$$P_{u,pl} = \tau \, l_g \, \pi \, \phi \tag{24}$$

$$P_{u,LEFM} = \sqrt{2 \, \overline{EA} \, G_{f,s} \, \pi \, \phi} \tag{25}$$

$$\overline{EA} = \left(\frac{1}{E_r A_r} - \frac{1}{E_w (A_w - A_r) + E_r A_r} \right)^{-1} \tag{26}$$

where indices pl and $LEFM$ denote plasticity theory and linear elastic fracture mechanics respectively. The indices r and w denote rod and wood and EA denotes the axial stiffness (the wood area A_w is the gross area $b \cdot h$). Assuming that a crack propagates from the free end of the rod, Eq. (25) can easily be derived using an energy release rate approach, see any standard textbook on fracture mechanics, e.g. [22].

For the case of $E_w(A_w - A_r) \gg E_r A_r$, Eq. (25) can be written:

$$P_u = \sqrt{2\, E_r A_r\, G_{f,s}\, \pi\, \phi} \tag{27}$$

or in terms of nominal shear strength:

$$f_v = P_u/(\pi \phi l_g) = k \lambda^{-0.5}\, l_g^{-0.5} \tag{28}$$

with k being a material constant $k = \sqrt{0.5 E_r G_{f,s}}$ and λ denoting the slenderness ratio $\lambda = l_g/\phi$. As expected, the FE-results coincide with the analytical expressions for the cases of extremely ductile and extremely brittle behaviour. In the transition region, however, there is a difference, and here the generalised Volkersen theory, Eq. (4), predicts results closer to the numerical results. The difference between Eq. (4) and the FE-results can be explained by the fact that Eq. (4) assumes the bondline to behave linear elastic during the complete course of loading. Furthermore Eq. (4) assumes a one-dimensional state of stress (pure shear) in the bondline and an axisymmetric geometry and loading. Since for the extreme values of ω, the FE-simulations and the analytical results coincide, the assumptions of a one-dimensional stress-state and axisymmetry do not seem to influence the results for the present geometry. For larger timber cross sections, however, the use of an analytical expression assuming axisymmetry, would probably have to involve some kind of effective wood cross-section.

4 Parameter Study II–Loading Conditions

4.1 Scheme

In this study, the influence of applying the load by pull-compression versus loading by pull-pull was studied for a number of different glued-in lengths and fracture energy values. The effect of using plates of different sizes and shapes was investigated: a 120 mm square plate, a 100 mm diameter circular plate and a 40 mm circular plate. There was a hole for the rod in all plates. This hole had a diameter equal to the hole in the wood plus 1 mm, i.e. 16+0.5+0.5+1.0=18 mm. For most of the simulations in this study, the

finite element discretisation used was essentially the same as the one reported previously. In order to check that this was appropriate for the contact modelling, a finer element mesh with more nodes and elements at the contact surfaces was also tested. In addition to giving results regarding the effect of load application, this study also gives some additional information about the effect of rod length and fracture energy. The various loading conditions were applied for two glued-in lengths (160 and 320 mm) and for three different values of $G_{f,s1}$ (1,2 and 4 kJ/m^2). As in the previous studies, it was assumed that $G_{f,s2} = G_{f,s1}$ and that $G_{f,n} = 0.2G_{f,s1}$. All other geometry and material parameters were according to simulation A1.

4.2 Results

The results from the simulations in terms of pull-out strengths are summarised in Table 3. Some of the parameter combinations used in this study coincide with those of study I, the corresponding simulations are given in parentheses. The general outcome of this parameter study is that the pull-compression case, as expected, always gives lower load-bearing capacity than the pull-pull case. This is because the pull-compression case results in a more non-uniform shear stress distribution than the pull-pull case. The capacity is approximately 10–20% lower in pull-compression for the case with the square plate and the large circular plate. For the small circular plate the load-bearing capacity is reduced by approximately another 10%. The reduction in capacity is more severe for the more brittle cases, i.e. the longer glued in lengths and lower fracture energies.

*Table 3: Predicted pull-out strength of glued-in rods. * indicates that a refined FE-mesh was used.*

Loading type	Plate type	$G_{f,s}$ N/m^2	l_g mm	P_{ult} kN
pull-comp.	□120	2000	320	73.3
pull-pull	-	2000	320	83.8
pull-comp.	ϕ100	2000	320	72.9
pull-comp.	□120	2000	160	50.3
pull-pull	-	2000	160	54.9
pull-comp.	□120	4000	320	90.9
pull-pull	-	4000	320	101.4
pull-comp.	□120	4000	160	60.8
pull-pull	-	4000	160	66.8
pull-comp.	□120	1000	320	53.4
pull-pull	-	1000	320	65.9
pull-comp.	□120	1000	160	41.3
pull-pull	-	1000	160	45.2
pull-comp.*	□120	2000	320	73.5
pull-comp.*	ϕ100	2000	320	72.7
pull-comp.*	ϕ40	2000	320	67.3

5 Conclusions

The following conclusions can be drawn from the present study:

- A nonlinear, 3-dimensional bondline model to simulate the behaviour of glued-in rods for timber structures by finite element analysis was developed.
- The model was tested for a wide range of material and geometrical properties and it was found that it includes the theories of perfect plasticity and linear elastic fracture mechanics as special cases.
- The fracture energy of the adhesive layer is an important parameter for the prediction of the ultimate load of glued-in rods.
- The model predicts an effect of size on the nominal shear strength of glued-in rods, a phenomenon known from the test results of several independent surveys.
- Loading the glued-in rod in pull-compression reduced the ultimate load by 10–20% compared with loading in pull-pull.

Acknowledgements

The GIROD project involves the following research institutes: SP – Swedish National Testing and Research Institute, FMPA Otto-Graf Institute (Germany), University of Karlsruhe (Germany) and TRADA Technology (UK) and Lund University. The financial support through grant no. SMT4-CT97-2199 by the European Commission (DG XII) and the co-operation from the partners involved in this research project are gratefully acknowledged. This research was also in part financially supported by the Swedish Council for Building Research (BFR), project no. 19960633. This support is also gratefully acknowledged.

References

[1] Aicher, S. and Herr J. *Bonded glulam-steel rod connections with long anchorage length.* Otto-Graf Journal Vol. 8. Forschungs und Materialprüfungsanstalt Baden-Württemberg. Stuttgart, Germany 1997.

[2] Riberholt, H. *Glued bolts in glulam.* Report R210, Department of Structural Engineering, Technical University of Denmark, Lyngby, Denmark 1986.

[3] Ehlbeck, J. and Siebert, W. *Praktikable Einleimmethoden und Wirkungsweisen von eingeleimten Gewindstangen unter Axialbelastung bei Übertragung von grossen Kräften und bei Aufnahme von Querzugkräften in Biegeträgern. Teil 1: Einleimmethoden/Messverfahren/Haftspannungsverlauf.* Forschungsbericht: Versuchsanstalt für Stahl, Holz und Steine, Abteilung Ingenieurholzbau, Universität Karlsruhe, Germany 1987.

[4] Deng, J.X. *Strength of Epoxy Bonded Steel Connections in Glue Laminated Timber.* PhD-thesis. Civil engineering research report 97/4. Dept. of Civil Engineering, University of Canterbury, Christchurch, New Zealand 1997.

[5] Aicher, S., Gustafsson, P. J. and Wolf, M. *Load displacement and bond strength of glued-in rods in timber influenced by adhesive, wood density, rod slenderness and diameter.* In Proceedings 1st RILEM Symposium on timber engineering, Stockholm. Ed. L. Boström. pp. 369–378. RILEM Publications S.A.R.L. Cachan, France 1999.

[6] Kangas, J. *Joints of glulam structures based on glued-in ribbed steel rods.* VTT Publications 196. Technical research centre of Finland. Espoo, Finland 1994.

[7] Korin, U. *Development of Embedding Loads of Rebars in GLULAM.* Proceedings of the 1997 Conference of IUFRO S5.02 Timber Engineering. Copenhagen, Denmark 1997.

[8] Kemmsies, M. *Comparison of Pull-out Strengths of 12 Adhesives for Glued-in Rods for Timber Structures.* SP REPORT 1999:20. SP Swedish National Testing and Research Institute, Building Technology. Borås, Sweden 1999.

[9] Riberholt, H. *Glued bolts in glulam – Proposal for CIB Code.* Proceedings CIB-W18/21-7-2. Meeting twenty-one. Parksville, Canada 1988.

[10] Aicher, S., Höfflin, L. and Wolf, M. *Influence of specimen geometry on stress distribution in pull-out tests of glued-in steel rods in wood.* Otto-Graf Journal Vol. 9. Forschungs und Materialprüfungsanstalt Baden-Württemberg. Stuttgart, Germany 1998.

[11] Johansson, C-J., Serrano, E., Gustafsson, P.J. and Enquist, B. *Axial strength of glued-in bolts. Calculation model based on non-linear fracture mechanics - A preliminary study.* Proceedings CIB-W18. Meeting twenty-eight. Copenhagen, Denmark 1995.

[12] Müller, J. and von Roth, W. *Untersuchungen zum Tragverhalten zur Faser in Nadelholz eingeleimte Stäben aus unterschiedlichen Materialen.* Holz als Roh und Werkstoff 1991;(49):85–90.

[13] Volkersen, O., *Die Nietkraftverteilung in Zugbeanspruchten Nietverbindungen mit Konstanten Laschenquerschnitten.* Luftfahrtforschung, 1938;(35):41–47.

[14] Gustafsson, P. J. *Analysis of generalized Volkersen-joints in terms of non-linear fracture mechanics.* In: Mechanical Behaviour of Adhesive Joints, pp. 323–338. Edition Pluralis, Paris, France 1987.

[15] Aicher, S., Wolf, M. and Dill-Langer, G. *Heat flow in a glulam joist with a glued-in steel rod subjected to variable ambient temperature.* Otto-Graf Journal Vol. 9. Forschungs und Materialprüfungsanstalt Baden-Württemberg. Stuttgart, Germany 1998.

[16] Guan, Z. W. *Structural behaviour of glued bolt joints using FRP.* Proceedings 5th World Conference on Timber Engineering, Vol. 1, pp. 265–272. Presses polytechniques et universitaires romandes, Lausanne, Switzerland 1998.

[17] Gustafsson, P. J. *Fracture mechanics studies of non-yielding materials like concrete: modelling of tensile fracture and applied strength analyses.* Report TVBM-1007, Lund Institute of Technology, Division of Building Materials, Lund , Sweden, 1985.

[18] Möhler, K. and Hemmer, K. *Eingeleimten Gewindstangen.* Bauen mit Holz 1981;83(5):296–98.

[19] Hibbitt, Karlsson & Sorensen, Inc. *ABAQUS, Version 5.7.* Pawtucket, RI, USA 1997.

[20] Wernersson, H. *Fracture characterization of wood adhesive joints.* Report TVSM-1006, Lund University, Division of Structural Mechanics 1994.

[21] Serrano, E. and Gustafsson, P. J. *Influence of bondline brittleness and defects on the strength of timber finger-joints.* Int J Adhesion and Adhesives. 1999;19(1):9–17.

[22] Hellan, K. *Introduction to fracture mechanics* McGraw-Hill Book Co. Singapore 1985.